

Acoustic and Visual Characteristics of Cavitation Induced by Mechanical Heart Valves

Kwanghyun Sohn¹, Keefe B. Manning¹, Arnold A. Fontaine¹, John M. Tarbell², Steven Deutsch¹

¹Department of Bioengineering, The Pennsylvania State University, University Park, PA, ²Department of Biomedical Engineering, The City College of New York, New York, NY, USA

Background and aim of the study: A sudden pressure drop and recovery can induce cavitation in liquids. Mechanical heart valves (MHVs) generate such a pressure drop at closure, and cavitation generation around MHVs has been demonstrated many times. Cavitation is suspected as being a cause of blood and valve material damage.

Methods: In this in-vitro experiment, visual images and acoustic signals associated with MHV cavitation were studied to reveal cavitation characteristics. Björk-Shiley Convex-Concave valves, one with a pyrolytic carbon occluder and one with a Delrin occluder, were installed in a single-shot valve chamber. Cavitation intensity was controlled by load (dP/dt) and air content of water. The acoustic signal was measured using a hydrophone and visual images

A sudden pressure drop and recovery in a liquid can generate cavitation (1). Cavitation is the process of growth and collapse of vaporous and gaseous bubbles in a liquid, and can be highly destructive. For example, it is well known that cavitation can erode the surface of hydraulic machinery (1) as a result of shock waves and liquid jets formed during bubble collapse.

During closure, the occluder movement of a mechanical heart valve (MHV) generates a sudden pressure drop by several mechanisms (2-4). It has been shown that cavitation can develop around MHVs in vitro (2,5-7), while the erosion of explanted valves and blood trauma of cardiac valve patients indicate the possibility of cavitation occurring in vivo (8-14).

The quantification of MHV cavitation intensity is necessary for the study of blood cell and valve material damage by cavitation. Cavitation in a clear liquid, such as water, can be monitored visually with a high-

speed video camera system.

Results: Cavitation images showed that 10 ppm water rarely developed cavitation, unlike the 16 ppm water. A distinct peak pressure was observed at cavitation collapse that was a good indicator of MHV cavitation intensity. The average of the peak pressures revealed that cavitation intensity increased faster with increasing load for the 16 ppm water.

Conclusion: The use of the peak pressure may be the preferred method for correlating cavitation intensity in structures for which the separation of valve closure noise and cavitation signal is difficult, as for the valves studied here.

The Journal of Heart Valve Disease 2005;14:551-558

speed video camera. However, in the case of cavitation in blood, the visual approach is not feasible due to the opacity of blood. An alternative choice is an acoustic approach, as cavitation is accompanied by a characteristic acoustic signal. However, one obstacle to the acoustic detection method is the fact that the cavitation signal can be mixed with the valve closure acoustic signal (15).

Garrison et al. (9) introduced the first acoustic method for the quantification of MHV cavitation intensity. These authors reported that the acoustic signal with cavitation showed high-frequency (35-350 kHz) components, whereas the acoustic signal without cavitation (valve closure) was restricted to lower frequencies. Zapanta et al. (16) applied this band pass filtering method to the correlation of valve dynamics and cavitation intensity. This group studied the effects of valve geometry (Medtronic-Hall and Björk-Shiley Monostrut), occluder material (pyrolytic carbon and Delrin) and gap width between the occluder and housing (tight and leaky).

Recently, Johansen et al. (15) developed a new method for cavitation evaluation. These authors hypothesized that cavitation is a random event in the

Address for correspondence:
Steven Deutsch PhD, The Pennsylvania State University,
Department of Bioengineering, 205 Hallowell Building, University
Park, PA 16802, USA

time domain, and its acoustic signal consists of high-frequency components. In contrast, valve closure has a regular pattern in the time domain, and its acoustic signal consists of mostly low-frequency components. According to this hypothesis, the ensemble average of the acoustic signal in the time domain removes the cavitation sound and reveals the valve vibration sound (deterministic signal). On the other hand, the ensemble average in the frequency domain will contain both cavitation and valve vibration sounds. Thus, the difference between the two averages (frequency and time domain ensemble averages) will reveal the cavitation signal (non-deterministic signal). It was reported that the non-deterministic signal energies showed a linear relationship with the root-mean square (RMS) values developed by Garrison et al. (9).

In the present study, both visual and acoustic cavitation characteristics were investigated. A Björk-Shiley Convex-Concave valve was installed in a single-shot valve chamber (17) filled with water. The air content and load (dP/dt) were controlled to set the cavitation level. Both a Delrin and a pyrolytic carbon occluder were tested, and the results of the study showed that a distinctive peak pressure accompanies the synchronous collapse of cavitation bubbles that may be a useful signature for detecting and quantifying cavitation.

Materials and methods

A single-shot valve chamber, intended to simulate the left side of the heart and the mitral valve closure dynamics, was built according to the specifications outlined by Chandran and Aluri (18). The chamber was constructed from transparent acrylic for cavitation image capture, and consisted of a ventricular chamber and an atrial chamber. The ventricular chamber was sealed and connected to a pneumatic driver that controlled chamber pressure. The atrial chamber was open to the atmosphere, and there was no atrial contraction simulation.

A Björk-Shiley Convex-Concave valve (size 29 mm) was mounted between the atrial and ventricular chambers. Two different occluder materials (pyrolytic carbon and Delrin) were evaluated. Since cavitation inception is substantially influenced by the number of nuclei and the dissolved air content (19,20), water was prepared with two different air contents: 16 ppm and 10 ppm. The 16 ppm water was tap water that had been stored in an open container for one day to remove over saturated air; the 10 ppm water was degassed under low pressure in a closed container. Air content was measured using a Van Slyke apparatus; this determines the total gas content of a liquid as the sum of the dissolved gas content and the free gas content.

The pneumatic driver simulated ventricular contrac-

tion by supplying high-pressure air over the liquid in the ventricular chamber. The rate of pressure increase in the ventricular chamber, dP/dt , was defined over the first 20 ms of the ventricular systolic period. After completion of systole and valve closure, the high pressure was released to simulate ventricular diastole, and the mitral valve opened.

Two types of experimental protocol were used in the present study. In the first case, three sets of 30 cycles of acoustic signals and four cycles of images were stored at each operating condition, as reported elsewhere (15). The acoustic signals and images were not synchronized. Thus, a total of 90 cycles of acoustic signals and 12 cycles of visual images were collected at each condition. This allowed the accumulation of sufficient data to permit statistical analysis. For the second protocol, synchronization between the visual and acoustic data was achieved which allowed the visual growth and collapse of cavitation to be correlated against the specific acoustic signature. Synchronization was performed during post processing.

For the non-synchronized data, the experimental instruments were arranged as shown in Figure 1 to obtain ventricular chamber pressure, atrial chamber pressure and cavitation images. The ventricular chamber pressure was measured with a Millar pressure catheter submerged in the chamber 50 mm horizontally and 25 mm vertically from the major orifice of the valve. The data were stored using an Iotech WaveBook digital data acquisition system for 3 s at a 20 kHz sampling rate. A range of loads (from 500 to 4,500 mmHg/s) was used to assess cavitation intensity. The

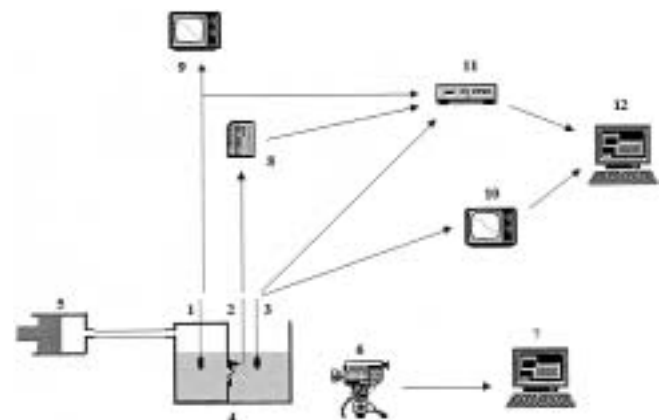


Figure 1: Layout for the initial experiment. 1) Pressure transducer (Millar, MPC-500); 2) accelerometer (PCB 352M66); 3) hydrophone (RESON, TC4038); 4) single-shot chamber; 5) pneumatic drive unit; 6) high-speed digital imaging system (Kodak Motion Corder Analyzer SR series); 7) PC; 8) signal conditioner (PCB ICP Sensor Conditioner 482A22); 9) oscilloscope (LeCroy 9310); 10) oscilloscope (LeCroy LT262); 11) digital data acquisition system (Iotech WaveBook 512A); 12) PC.

atrial chamber pressure was measured using a 1 MHz hydrophone (Reson Inc.), amplified by 20 dB and band pass-filtered from 35 kHz to 300 kHz. The hydrophone has a diameter of 4 mm and a length of 58 mm, and was positioned 25 mm horizontally, and vertically, from the center of the valve and 25 mm into the ventricular chamber. Thirty cycles of the atrial pressure during valve closure, from 1 ms before valve closure to 4 ms after valve closure, were recorded at a sampling rate of 1 MHz on a LeCroy oscilloscope. A Kodak SR-Ultra Motion Corder Analyzer was used to acquire high-speed digital images of MHV cavitation at 3,000 frames per second (fps).

For the synchronized data, some layout changes were necessary (see Fig. 2). The sampling rate of the acoustic signal was sufficient to satisfy the Nyquist criterion to record more precise acoustic signal information. For the synchronization of the acoustic signal and the visual images, a function generator provided a sawtooth signal that was digitized using a Kodak Multi-Channel Data Link. By employing this sawtooth signal, the time of image capture could easily be synchronized with the high-frequency acoustic signal.

Results and discussion

Images of the cavitation for the non-synchronization method are displayed in Figure 3. The cavitation intensity of the 16 ppm water (Fig. 3a, left column) increased around the major orifice of the valve as the load increased, as expected. With the pyrolytic carbon occluder, there was no visible cavitation at 500 mmHg/s, occasional cavitation at 2,500 mmHg/s, frequent cavitation at 3,500 mmHg/s, and persistent cavitation at 4,500 mmHg/s. The pyrolytic carbon occluder generated bubble cavitation with occasional weak cloud (vortex) cavitation. At higher loads, the

bubble cavitation was distributed over a wider area in front of the major orifice of the occluder. The Delrin occluder (Fig. 3b, left column) showed no visible cavitation at 500 mmHg/s, occasional cavitation at 2,500 mmHg/s, and persistent cavitation at 3,500 mmHg/s. No data were acquired at 4,500 mmHg/s for the Delrin occluder because cavitation was consistent at the 3,500 mmHg/s. This occluder generated predominantly cloud cavitation that was distributed in an arc shape around the occluder tip. The cloud cavitation may appear weaker in visual images than in actuality because the background provided by the white Delrin occluder limited optical contrast. With the 16 ppm water, the occluders illustrated different cavitation development in response to the loads applied, suggesting that different mechanisms for cavitation may be responsible. The 10 ppm water rarely generated cavitation for either occluder (Fig. 3a and b, right columns). For example, at 4,500 mmHg/s with the pyrolytic carbon occluder, the 16 ppm water generated cavitation every cycle, but the 10 ppm water generated cavitation only occasionally. Fewer nuclei were present in the 10 ppm water, thereby limiting cavitation formation and requiring a higher pressure drop to induce cavitation. Larger nuclei may be present with the 16 ppm water, resulting in a lower pressure drop required for cavitation.

Representative acoustic signals of the non-synchronized data are displayed in Figure 4, where '0' in the time axis denotes the instant of valve impact. At the low load conditions, the two water samples showed the same acoustic signal patterns, but at the high load conditions the acoustic signatures were different from moderate to high loads. The 10 ppm water usually did not generate visible cavitation, and the acoustic signal was flat. Unlike the 10 ppm water, there was a significant increase in peak pressure with increasing load for the 16 ppm water. According to the acoustic signal of the 10 ppm water (see Fig. 4, right column), the valve vibration signals (no visible cavitation was imaged) of both occluders increased as the load increased, with major differences in magnitudes between the occluders. The valve vibration signal may be dependent on the occluder material properties (see Table I). The heavy, rigid pyrolytic carbon occluder generated a very strong valve vibration signal, whilst the light, flexible Delrin occluder generated a very weak signal.

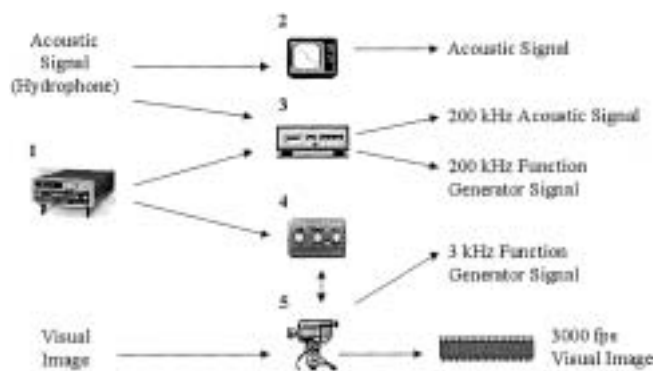


Figure 2: Layout for synchronization experiment. 1) Function generator; 2) oscilloscope (LeCroy 9310); 3) digital data acquisition system (Iotech WaveBook 512A); 4) Kodak Multi-channel Data Link; 5) high-speed digital imaging system (Kodak Motion Corder Analyzer SR series).

Table I: Occluder material properties.

Material	Pyrolytic carbon	Delrin
Density (kg/m ³)	2,480	1,430
Modulus of elasticity (GPa)	27.6	3.10

The difference between the 16 ppm water and the 10 ppm water acoustic signals revealed the cavitation signal at high load conditions.

Two different acoustic signals, one with and the other without cavitation, under exactly the same load were compared directly in Figures 5 and 6 for the pyrolytic carbon occluder and the Delrin occluder, respectively. Each figure contains high-speed videography images (3,000 fps) with and without cavitation,

and their respective pressure signals. In the case of the pyrolytic carbon occluder (Fig. 5), which produced bubble cavitation primarily, the two acoustic signals (cavitating and non-cavitating) were similar over the entire observation period except around the peak pressure in the cycle with cavitation. The difference between the two acoustic signals with and without cavitation for the Delrin occluder was associated with cloud cavitation. Cloud cavitation usually generated a

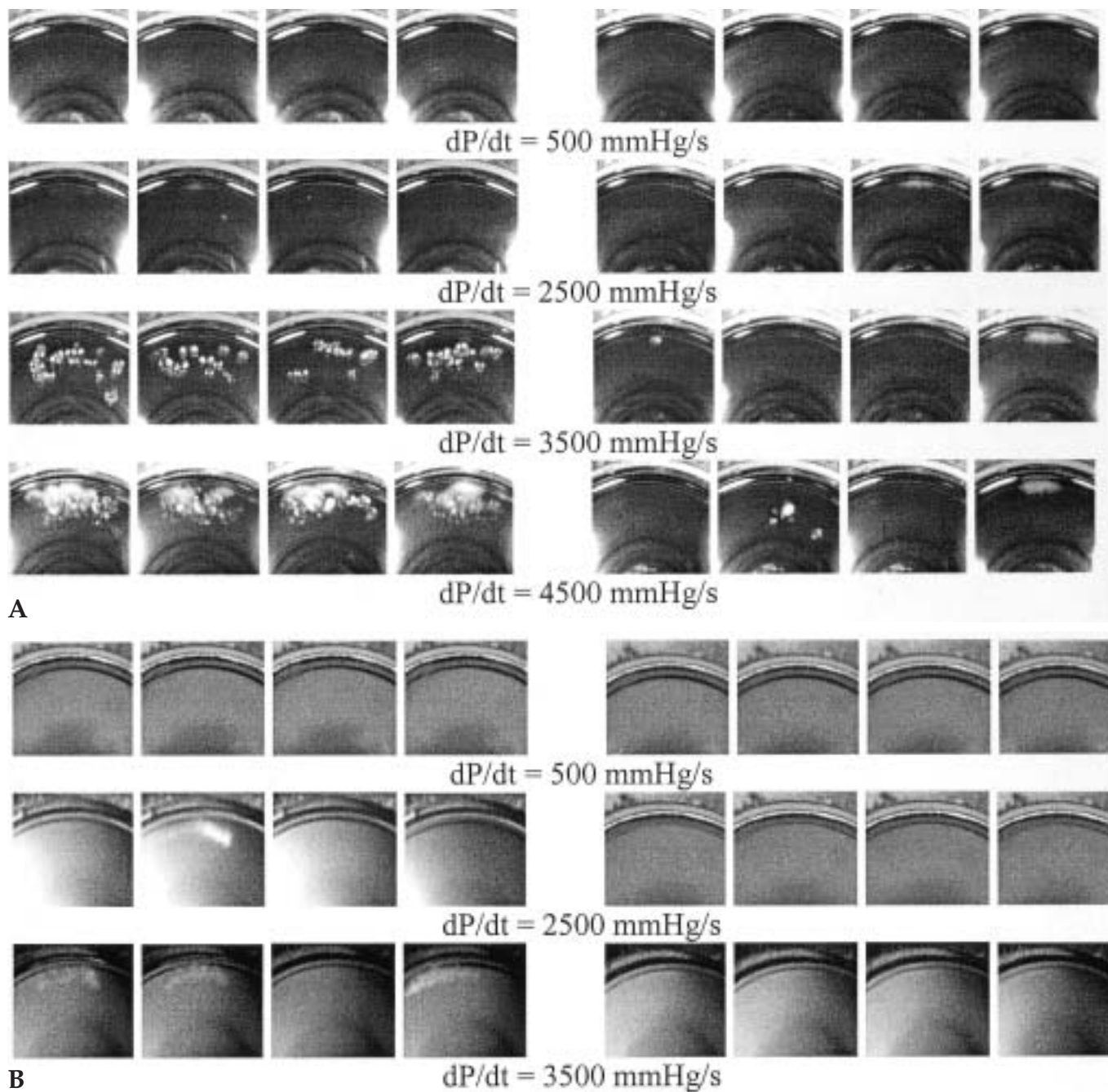


Figure 3: Cavitation images at each condition; the largest cavitation image was selected for each cycle. a) Pyrolytic carbon occluder (left column: 16 ppm air, right column: 10 ppm air); b) Delrin occluder (left column: 16 ppm air, right column: 10 ppm air).

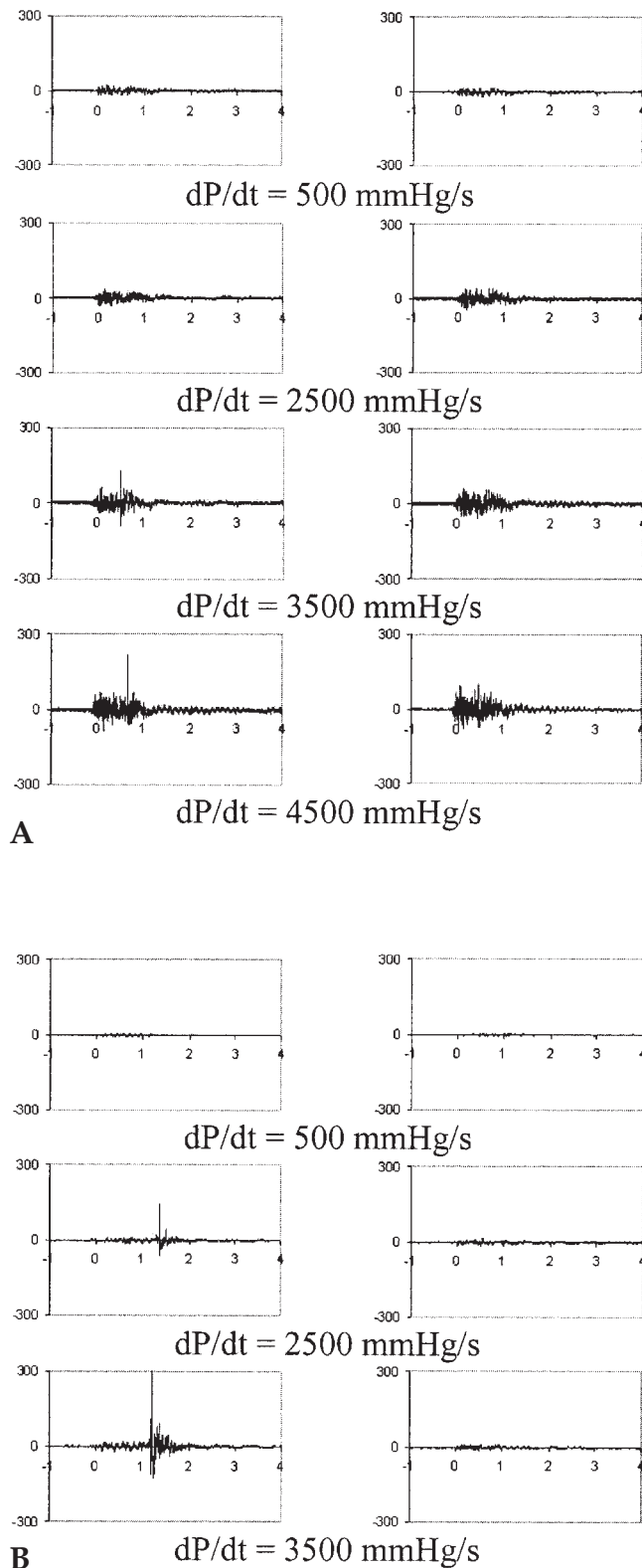


Figure 4: Acoustic signals for each condition (y-axis = Pressure (mmHg)). a) Pyrolytic carbon occluder (left column: 16 ppm air, right column: 10 ppm air); b) Delrin occluder (left column: 16 ppm air, right column: 10 ppm air).

very strong peak pressure, followed by multiple pressure fluctuations. As illustrated in Figures 5 and 6, there was a clear difference in pressure signals between the cavitating and non-cavitating conditions at the same loads for the bubble and cloud cavitation shown with the pyrolytic carbon occluder and Delrin occluder, respectively. There was much more evidence of significant energy in the pressure signal associated with cloud cavitation than with bubble cavitation.

Using the synchronized method to check the timing of the peak pressure, five successive images captured at 3,000 fps were marked as five small circles on the time axis of the acoustic signal (Fig. 7). Figure 7a shows the peak pressure timing for the pyrolytic carbon occluder at 4,500 mmHg/s in the 16 ppm water, while Figure 7b illustrates the Delrin occluder at 4,500 mmHg/s in the 10 ppm water. The five successive visual images show cavitation growth and collapse, even though 3,000 fps was insufficient to display the process in detail. According to the visual images of the pyrolytic carbon occluder, the cavitation bubbles grew together and collapsed together, and the peak pressure occurred between the maximum bubble growth and disappearance of cavitation. This suggested that the peak pressure was caused by cavitation collapse. The peak pressure of the Delrin occluder also occurred during maximum growth and final collapse of cavitation. The visual images showed the cloud cavitation behavior, though the motion of individual tiny bubbles was not detectable. Wang and Brennen (21-23) suggested the possibility of synchronous collapse of cloud cavi-

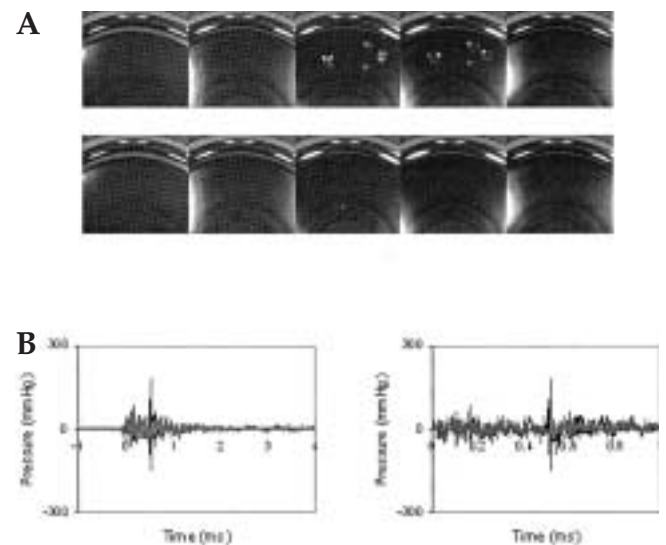


Figure 5: Sound signal comparison between two cycles for the pyrolytic carbon occluder (10 ppm air in water, $dP/dt = 5,000$ mmHg/s) with and without cavitation. a) Cavitation images (each row shows successive images taken at 3,000 fps); b) pressure signal traces (dark curve: with cavitation, light curve: without cavitation).

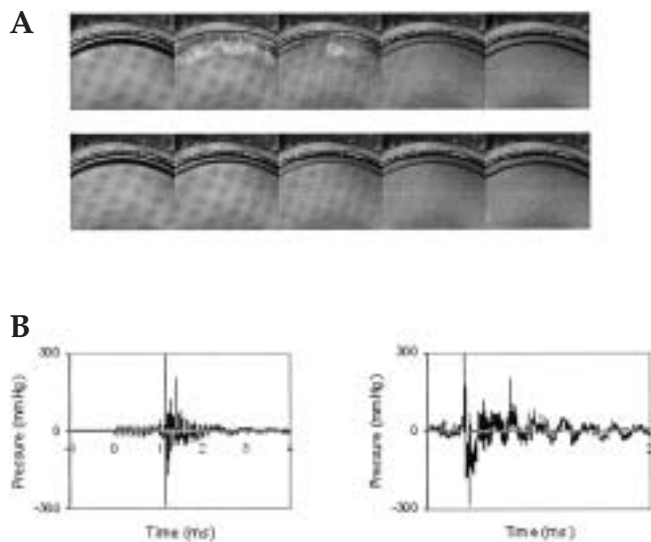


Figure 6: Sound signal comparison between two cycles for the Delrin occluder (10 ppm degassed water, $dP/dt = 5,000$ mmHg/s) with and without cavitation. a) Cavitation images (each row shows successive images taken at 3,000 fps); b) pressure signal traces (dark curve: with cavitation, light curve: without cavitation).

tion. These authors found that the cloud interaction parameter $\beta = \alpha_0 (1 - \alpha_0) A_0^2 / R_0^2$, where α_0 denotes the void fraction of the cloud, A_0 is the initial radius of the cloud, and R_0 is the initial radius of the bubbles within the cloud, is important for characterizing the cavitation dynamics. In the case of large β , the bubbles interact and collapse nearly simultaneously. Bubbles on the surface of a cloud collapse first, and an inward propagating shock wave is formed and focused at the cloud center during the collapse, and extremely high pressure near the center is generated (24,25). With the synchronized data, the measured peak pressure occurs within the resolution of visual bubble collapse using 3,000 fps.

To check the relationship between the RMS and peak pressures with cavitation intensity, the RMS and peak pressure values for each cycle were determined, and the 30 values were averaged for each. Figures 8 and 9 show the average RMS and peak pressures for the pyrolytic carbon occluder and the Delrin occluder, respectively. In Figure 8a, the RMS pressures for the 10 and 16 ppm water are nearly identical during all conditions. However, a separation of the 16 ppm water from the 10 ppm water (Fig. 8b) occurred when peak pressures were calculated. The peak pressures for the 10 ppm water did not remain flat but increased similar to the 16 ppm water. This suggests that the peak pressure may be a better indicator of cavitation intensity for the pyrolytic carbon occluder. In Figure 9a, the RMS pressure increased much faster for the 16 ppm

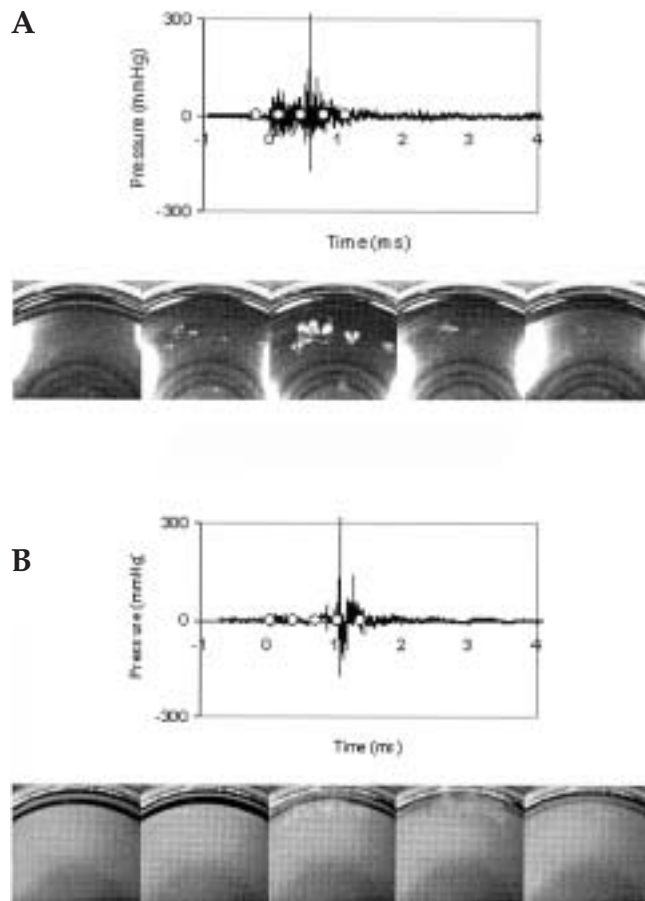


Figure 7: Timing of the peak pressure with: a) the pyrolytic carbon occluder (16 ppm air, 4,500 mmHg/s); and b) the Delrin occluder (10 ppm air, 4,500 mmHg/s), where each sequential image is represented by a circle on the trace.

water compared to the 10 ppm water with increasing load. At a non-cavitating load, the RMS values were virtually identical, as could be similarly said with the peak pressures. The peak pressures (Fig. 9b) for the 16 ppm water illustrated a similar trend with increasing load. However, the 10 ppm water did not show an increase in peak pressures with increasing load but rather was flat. The difference of the peak pressures between the two water samples for both occluders was indicative of the increased cavitation intensity for the 16 ppm water over the 10 ppm water, but the difference of the RMS pressures between the two water samples was indicative of increased cavitation intensity only for the Delrin occluder.

In conclusion, acoustic signals and visual images of MHV cavitation were studied using a single-shot valve chamber with the Björk-Shiley Convex-Concave valve. A pyrolytic carbon occluder and a Delrin occluder were tested with cavitation intensity controlled by load (dP/dt) and air content of water.

The pyrolytic carbon occluder generated mainly

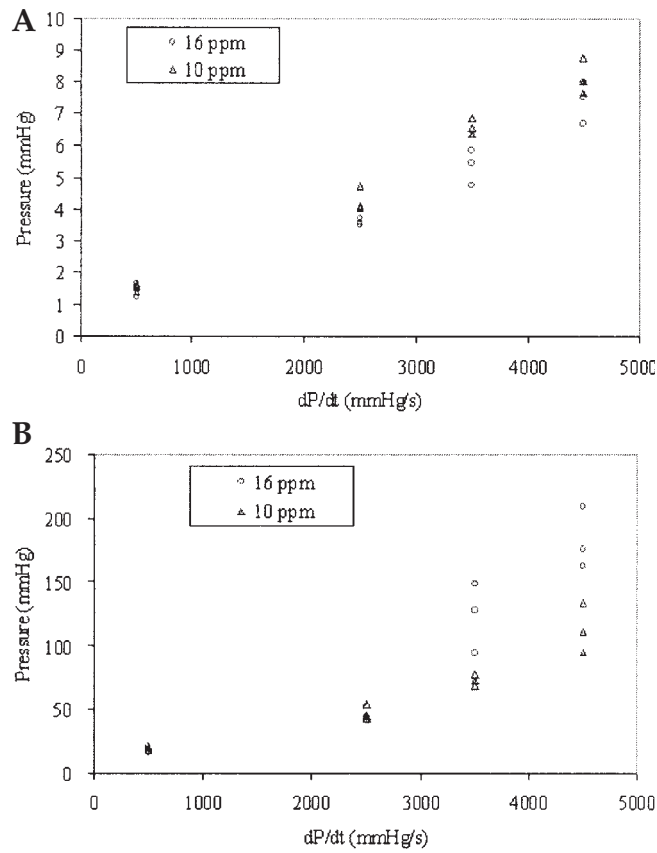


Figure 8: 10 and 16 ppm air in water comparison with the pyrolytic carbon occluder. a) RMS pressure; b) Peak pressure.

bubble cavitation, and the cavitation bubbles grew and collapsed in phase. There were instances of some cloud cavitation at higher loads. The Delrin occluder generated cloud cavitation predominantly, and the tiny bubbles of the cloud cavitation appeared to behave synchronously. The 10 ppm water generated little or no cavitation with increasing load, unlike the 16 ppm water which showed cloud cavitation with increasing load. Peak pressure and RMS pressure, which has been shown to be a good measure of cavitation intensity for Delrin occluders (9), distinguish from non-cavitating conditions for the Delrin occluder (cloud cavitation), but only peak pressure provides discrimination for the pyrolytic carbon occluder (bubble cavitation). Therefore, the use of the peak pressure may be the preferred method for correlating cavitation intensity in structures for which the separation of valve closure noise and cavitation signal is difficult, as for the pyrolytic carbon valve studied here. Such peak pressures, which are quite temporally distinct from valve closure, are readily available with the use of high-frequency hydrophones.

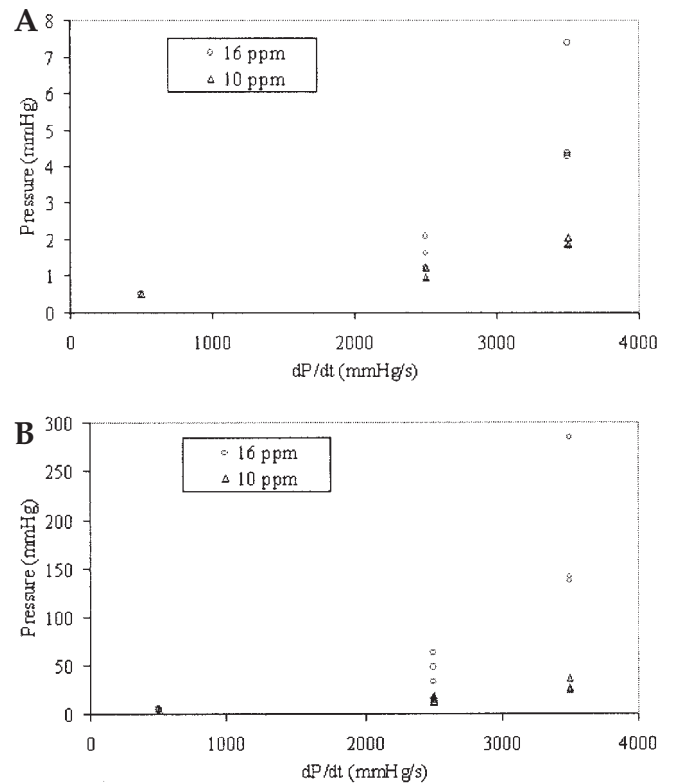


Figure 9: 10 and 16 ppm air in water comparison with the Delrin occluder. a) RMS pressure; b) Peak pressure.

Acknowledgements

These studies were supported by NIH (grant no. HL 48652).

References

1. Young FR. Cavitation. Imperial College Press, London, 1999
2. Stinebring DR, Lamson TC, Deutsch S. Techniques for in vitro observations of cavitations in prosthetic heart valves. In: Proceedings of the ASME 1991 Cavitation and Multiphase Flow Forum, Portland, Oregon, FED-Vol. 109, 1991:119-124
3. Garrison L. Hemolytic effects of chemical additives, aortic pressure changes, and cavitation in two new mock circulatory loops driven by the Penn State Ventricular Assist Device. PhD Thesis, The Pennsylvania State University, 1994
4. Makhijani VB, Yang HQ, Singhal AK, Hwang NH. An experimental-computational analysis of MHV cavitation: Effects of leaflet squeezing and rebound. J Heart Valve Dis 1994;3:535-548
5. Zapanta CM, Liszka EG, Lamson TC, et al. A method for real-time in vitro observation of cavit-

- tion on prosthetic heart valves. *ASME J Biomech Eng* 1994;116:460-468
6. Chandran KB, Lee CS, Chen LD. Pressure field in the vicinity of mechanical valve occluders at the instant of valve closure: Correlation with cavitation initiation. *J Heart Valve Dis* 1994;3:565-576
 7. Graf T, Reul H, Detlefs C, Wilmes R, Rau G. Causes and formation of cavitation in mechanical heart valves. *J Heart Valve Dis* 1994;3:549-564
 8. Lamson TC, Rosenberg G, Geselowitz DB, et al. Relative blood damage in the three phases of a prosthetic heart valve flow cycle. *Am Soc Artif Intern Organs J* 1993;39:M626-M633
 9. Garrison LA, Lamson TC, Deutsch S, Geselowitz DB, Gaumond RP, Tarbell JM. An in vitro investigation of prosthetic heart valve cavitation in blood. *J Heart Valve Dis* 1994;3:S8-S22
 10. Kafesjian R, Howanec M, Ward GD, Diep L, Wagstaff LS, Rhee R. Cavitation damage of pyrolytic carbon in mechanical heart valves. *J Heart Valve Dis* 1994;3:52-57
 11. Richard G, Beavan A, Strega P. Cavitation threshold ranking and erosion characteristics of bileaflet heart valve prostheses. *J Heart Valve Dis* 1994;3:S94-S101
 12. Paulsen PK, Jensen BK, Hasenkam JM, Nygaard H. High-frequency pressure fluctuation measured in heart valve patients. *J Heart Valve Dis* 1999;5:482-486
 13. Dexter EU, Aluri S, Radcliffe RR, et al. In vivo demonstration of cavitation potential of a mechanical heart valve. *Am Soc Artif Intern Organs J* 1999;45:436-441
 14. Levy DJ, Child JS, Rambod E, Gharib M, Milo S, Reisner SA. Microbubbles and mitral valve prostheses - transesophageal echocardiographic evaluation. *Eur J Ultrasound* 1999;10:31-40
 15. Johansen P, Manning KB, Tarbell JM, Fontaine AA, Deutsch S, Nygaard H. A new method for evaluation of cavitation near mechanical heart valves. *ASME J Biomech Eng* 2003;125:663-670
 16. Zapanta CM, Stinebring DR, Deutsch S, Geselowitz DB, Tarbell JM. A comparison of the cavitation potential of prosthetic heart valves based on valve closing dynamics. *J Heart Valve Dis* 1998;7:655-667
 17. Kini V, Bachmann C, Fontaine A, Deutsch S, Tarbell JM. Flow visualization in mechanical heart valves: Occluder rebound and cavitation potential. *Ann Biomed Eng* 2000;28:431-441
 18. Chandran KB, Aluri S. Mechanical valve closing dynamics: Relationship between velocity of closing, pressure transience, and cavitation initiation. *Ann Biomed Eng* 1997;25:926-938
 19. Green SI. Correlating single phase flow measurements with observations of trailing vortex cavitation. *J Fluids Eng* 1991;113:125-129
 20. Chambers SD, Bartlett RH, Ceccio SL. Determination of the in vivo cavitation nuclei characteristics of blood. *Am Soc Artif Intern Organs J* 1999;45:541-549
 21. Wang YC. Shock waves in bubbly cavitating flows. PhD Thesis, California Institute of Technology, 1996
 22. Wang YC, Brennen CE. The noise generated by the collapse of a cloud of cavitation bubbles. In: *ASME/JSME Symposium on Cavitation and Gas-Liquid Flow in Fluid Machinery and Devices*, FED-226, 1995:17-29
 23. Wang YC, Brennen CE. Shock wave development in the collapse of a cloud of bubbles. In: *ASME Cavitation and Multiphase Flow Forum*, FED-194:1994:15-20
 24. Blake JR, Keen GS, Tong RP, Wilson M. Acoustic cavitation: The fluid dynamics of non-spherical bubbles. *Philos Trans Roy Soc London Series A*, 1999;357:251-267
 25. Matsumoto Y. Bubble and bubble cloud dynamics. In: *Lauterborn W, Kurz T, eds. Nonlinear Acoustics at the Turn of the Millennium*. American Institute of Physics, Melville, NY, 2000:65-74